A graphene nanoribbon network and its biosensing application

Dong, Xiaochen; Long, Qing; Wang, Jing; Chan-Park, Mary B.; Huang, Yinxi; Huang, Wei; Chen, Peng

2011

Dong, X., Long, Q.,Wang, J., Chan-Park, M. B., Huang, Y., Huang, W. & Chen, P. (2011). A graphene nanoribbon network and its biosensing application. Nanoscale, 3(12), 5156-5160.

https://hdl.handle.net/10356/99887

https://doi.org/10.1039/C1NR11006C

A graphene nanoribbon network and its biosensing application

Xiaochen Dong[a], Qing Long[a], Jing Wang[b], M. B. Chan-Park[b], Yinxi Huang[b], Wei Huang [a]* and Peng Chen [b]*

[a] Key Laboratory for Organic Electronics & Information Displays (KLOEID) and Institute of Advanced Materials (IAM), Nanjing University of Posts and Telecommunications (NUPT), 9 Wenyuan Road, Nanjing, China, 210046

[b] School of Chemical and Biomedical Engineering, Nanyang Technological University, Singapore, 637457

Correspondence to: iamwhuang@njupt.edu.cn or chenpeng@ntu.edu.sg

Graphene oxide nanoribbons (GONRs) have been prepared by chemically unzipping multiwalled carbon nanotubes (MWCNTs). Thin-film networks of GONR were fabricated by spray-coating, followed by chemical or thermal reduction to form reduced graphene oxide nanoribbons (rGONRs). Raman spectroscopy and X-ray photoelectron spectroscopy (XPS) characterizations indicate that the thermal reduction in the presence of ethanol vapor more effectively restore the graphitic structure of GONR as compared to chemical reduction with hydrazine vapor. Electrical measurement under liquid-gate configuration demonstrates that rGONR network field-effect transistor exhibits much higher on/off ratio than that of a network of microsized reduced graphene oxides (rGOs) or that of a continuous film of single-layered pristine or chemical vapor deposition (CVD) grown graphene film. Furthermore, we demonstrated the potential applications of rGONR network for biosensing, specifically, real-time and sensitive detection of adenosine triphosphate (ATP) molecules.

Introduction

Graphene, a two-dimensional monolayer of carbon atoms packed into a honeycomb lattice, have attracted tremendous attentions because of their extraordinary electrical, physical, and chemical properties [1-4]. It holds a great promise for many applications, such as, nanoelectronics [5-6], sensors [7-13], transparent electrodes [14-15], supercapacitors [16-17], hydrogen storage [18-19], nanocomposites [20-21]. The fact that graphene is a zero band-gap semi-metal, however, largely limits its applications in nanoelectronics.

It has been discovered that the energy band-gap of graphene can be opened by reducing the width of graphene sheet to nanoscale in the form termed as graphene nanoribbons (GNRs) [22]. Several approaches have been developed to produce GNRs, including chemical vapor deposition on metallic nanowires [23], surface-assisted epitaxial growth [24], and e-beam lithography [25-26]. However, these methods are not scalable and of low-throughput. Alternatively, GNRs can be mass-produced in solution by electrochemically or chemically unzipping carbon nanotubes [27-29]. In this work, we longitudinally unzipped multi-walled carbon nanotubes by oxidation with strong acids to produce graphene oxide nanoribbons (GONRs). After thermal reduction in the presence of ethanol vapour to effectively restore the damaged carbon lattice, reduced graphene oxide nanoribbons (rGONRs) were obtained. Several groups have demonstrated the potential of single GNR for nanoelectronics [30-31]. Here, we fabricate and characterize the thin-film network field-effect transistors based on rGONRs and demonstrate its application for biosensing.

Experimental procedures

Materials

Multi-walled carbon nanotubes (MWCNTs) were obtained from Chengdu Organic Chemical Co. Ltd. H_2SO_4, $KMnO_4$, H_2O_2, HCl, hydrazine hydrate and ATP were all analytical grade and purchased from Sigma-Aldrich.

Preparation of GONRs

GONRs were prepared by chemically unzipping MWCNTs similarly to the previously reported [30]. Briefly, 50 mg MWCNTs were suspended in 10 ml H_2SO_4 for 1 hour. Then 250 mg $KMnO_4$ was added and the solution was heated at 60 ^oC for two hours. After the reaction, the products were poured into 200 ml cooled ice water containing 5 ml of 30% H_2O_2. At last, the mixture was vacuum filtrated through a PTFE membrane (5.0 μm pore size) to obtain GONR powder.

Reduction of GONR to rGONR and Fabrication of thin-film network devices

GONR thin-film network patterns (0.5×0.05 cm) were deposited on Si/SiO_2 substrates by spray-coating aqueous dispersion of GONRs (1mg/mL). Subsequently, the GONRs were reduced to rGONRs by hydrazine vapor (80 ^oC, overnight) or by thermal reduction with ethanol at 800, 900 or 1000 ^oC for 2 h [32], respectively. In the process of thermal reduction, ethanol vapor was brought into the reaction tube as hydrogen gas bubbled through the ethanol liquid [33-34]. Then, the source and drain electrodes were prepared at the two ends of rGONRs pattern with conductive silver paint. At last, the electrodes were insulated with silicone rubber and form a recording chamber.

Characterizations

UV-vis absorption (UV-2501, Shimadzu), Raman spectroscopy using the laser wavelength of 488 nm (CRM200 confocal Raman spectrometer, WITec), X-ray photoelectron spectroscopy (XPS, Kratos Axis Ultra DLD spectrometer, Al Ka radiation), scanning electron microscopy (SEM,

Sirion 200, JEOL), and transmission electron microscopy (TEM, JEM-2010, JEOL) were used to characterize the samples. The electrical characterization and detection measurement of rGONR thin-film devices configured as field-effect transistor were performed using a semiconductor device analyzer (Agilent, B1500A).

Electrical detection of ATP molecules

In the ATP detection experiments, 100 μL phosphate buffer saline (PBS, PH=7.2) solution was added into the recording chamber, in which Ag/AgCl reference electrode was immersed to apply gate voltage of V_g = 0 V. ATP molecules were added to defined final concentrations while the current of rGONR device at the voltage bias of V_d= 0.5 V was continuously monitored at the sampling frequency of 100 HZ using the semiconductor device analyzer (Agilent, B1500A).

Results and discussion

Fig. 1 shows the UV-vis absorbance spectra of MWCNTs and GONRs. The spectrum of MWCNTs presents an obvious absorption peak at ~260 nm. In contrast, in GONR spectrum the absorption peaks at ~230 nm, which is coincident with the absorbance spectrum of graphene oxide reported in the literature [35]. These observations imply that MWCNTs have been thoroughly oxidized and transformed into graphene oxide nanoribbons.

The morphology of the MWCNTs and the GONRs were characterized with SEM and TEM. SEM analyses reveal that the diameter of the MWCNTs is about 30-50 nm as shown in Fig. 2a. In comparison, the width of the GONRs is larger (50-100 nm) (Fig. 2b), indicating that the MWCNTs have been longitudinally opened by the treatment of H_2SO_4 and $KMnO_4$ (Fig. 2b, inset). As expected, the length of GONRs is similar to that of MWCNTs. To further confirm the unzipping of MWCNTs, we used TEM to examine the morphology of MWCNTs and the GONRs.

Under TEM, the expected hollow core of MWCNTs is cleared resolved (Fig. 2c), whereas GONRs (or rGONRs) appear as ribbon structure without hollow core (Fig. 2d). The high-resolution TEM images of MWCNT also clearly shows a crystal structure and hollow core (Fig. 2e), whereas the carbon structure of GONR is apparently impaired (Fig. 2f). These observations further confirm the unzipping of MWCNTs into GONRs.

To restore the oxidation induced damage on the carbon lattice, the GONRs were chemically reduced with hydrazine vapor at 80 ^{o}C or thermally reduced at different temperatures in the presence of ethanol vapor, respectively. The reduced GONRs (rGONRs) were characterized with Raman spectroscopy, in comparison with the Raman spectra of GONRs and MWCNTs. As shown in Fig. 3, the Raman spectrum of GONRs displays two prominent peaks at ~1350 and ~1630 cm^{-1}, corresponding to the well-recognized D and G bands, respectively [36]. In addition, the 2D band (at ~1350 cm^{-1}) observed in MWCNT spectrum disappeared due to oxidation. After the reduction with hydrazine vapor, the Raman spectrum of the resulting rGONRs exhibits un-shifted D and G bands, while the intensity ratio of these two bands (D/G) increases in comparison with that of GONR spectrum (from 1.03 to 1.12), indicating the restoration of sp^2 bonded carbon lattice [37]. As evidenced by the increased D/G ratio and in consistent with the report by Su et al. [32], reduction at high temperature in presence of ethanol vapor more efficiently restore the graphitic structure in rGONR, perhaps because the OH radicals decomposed from ethanol facilitate removal of oxygen-containing groups. A higher reduction temperature accelerates the thermal annealing of graphitic structure, and makes it easier for removing hydroxyls at the edges of the graphene oxides which requires a higher energy than dehydroxylation in the basal plane [38]. So, with the increase of reduction temperature, the D/G intensity ratio further increases to 1.53 at 1000 ^{o}C, suggesting

the effective conversion of sp^3 carbon domains to sp^2 domains. The effective recovery of carbon lattice at high temperatures (900 or 1000 ^oC) is further evidenced by the appearance of 2D band which is a characteristic peak observed in pristine or CVD grown graphene and not observed in GNORs and hydrazine vapor reduced GONRs. In addition, the Raman spectra of rGNORs shows an obvious left-shift of 2D and G band compared to that of MWCNTs owing to the doping effects of the oxygen containing groups [36].

The chemical attribute of the GONRs and rGONRs was analyzed by XPS, as shown in Fig. 4. In the XPS spectrum of the GONRs, there are four distinct peaks at 284.6, 286.6, 287.8, and 288.8 eV, corresponding to C=C/C-C in aromatic rings, C-O (epoxy and alkoxy), carbonyl, and carboxyl groups, respectively [39]. The amplitude of C-O peak is large, suggesting that the oxygen containing groups on GONRs are abundant. After the reduction with hydrazine vapor, the XPS spectrum of rGONRs also exhibits a much decreased C-O peak. On the other hand, an obvious C=N peak at ~287.0 eV appears due to the introduction of nitrogen by hydrazine reduction [6]. For the rGONRs reduced with ethanol vapor at 1000 ^oC, the C-O peak is further reduced, and the C=N peak and C-O/C=O peak are almost absent in the XPS spectrum. In agreement with Raman characterizations, it is evidenced that high temperature reduction with ethanol is more effective to recover the properties of GONRs, producing higher D/G ratio and lower oxygen containing groups. Ethanol has been used as a carbon source for chemical vapor deposition growth of carbon nanotubes and graphene [33,40]. In the high-temperature reduction process, it facilitates repair of the defects in graphitic structure. In addition, the OH radicals decomposed from ethanol at high temperature are able to attack carbon atoms with a dangling bond and prevent formation of amorphous carbon [41].

To investigate the electrical properties of the rGONR thin-film network, it is configured as liquid-gated field-effect transistor (Fig. 5a) which exhibits much higher transconductance as compared to commonly used back-gate configuration because of the thin thickness (<1 nm) of the electric double layer (gate layer). The transfer function (source-drain current vs. gate voltage, I_d-V_g) of a typical rGONR thin-film device is shown in Fig. 5b. It is noteworthy from the transfer function that the on-off ratio of our rGONR thin-film is much higher than that of a continuous film of single-layered pristine [42] or CVD grown graphene [9], or that of a thin-film network of reduced graphene oxides (rGOs) [43]. Specifically, the on-off ratio of our rGONR thin-film is ~52.0 +/- 8.6 (n=10 devices) while the on-off ratio of graphene sheet or rGO thin-film is typically <3 as reported in the literature [42,44]. And as anticipated, the MWCNT thin-films similarly prepared as the rGONR thin-films exhibit no obvious field-effect (on-off ratio) because of the metallic nature of MWCNTs. Therefore, the energy bad-gap is opened when MWCNTs are unzipped to nanoribbons. It has been demonstrated recently that the charge transport in the disordered graphene nanoribbons (rGONR here) is dominated by localized states, which lead to voltage-dependent electron-hopping and bandgap behavior [45-46]. The I_d-V_d curve of rGONR thin-film device is linear (Fig. 5b inset), indicating the good electrical contact between rGONR and metal electrodes and between rGONR flakes.

In a previous study [47], we used thin-film network of single-walled carbon nanotubes (SWCNTs) to detect of ATP molecules released from astrocytes. Pristine graphene and reduced graphene oxides have been expected as the unique or better alternative to SWCNT for sensor applications [43, 48-49]. To illustrate the ability of rGONR thin-film in biosensing and compare with SWCNT thin-film device, we investigated the detection properties of ATP molecules by our rGONR devices. As

shown in Fig. 6a-c, addition of ATP molecules caused clear conductance (thus current) decrease of rGONR thin-film. Notably, the detection limit achieved by rGONR devices is about 5 μM, which is 2 orders lower than that of SWCNT thin-film network (500 μM). The superior biosensing capability of rGONR thin-film may be attributed to two reasons: 1) SWCNT thin-film network is unavoidably plagued by the presence of metallic SWCNTs; 2) charge transport in rGONRs is dominated by the local states dispersed in rGONRs and its edges, therefore, is highly sensitive to the local molecular gating. Peculiarly, the current responses of rGONR and SWCNT are opposite, suggesting distinct sensing mechanisms. We previously proposed that electrostatic gating (field-effect) by the highly negatively charged ATP molecules caused increase of SWCNT conductance. To understand the detection by rGONR, we measured the I_d-V_g curve of rGONR thin-film device before and after addition of ATP. As seen in Fig. 6d, it is likely that ATP causes conductance decreases of rGONR through n-doping effect which suppresses hole density at the working point of V_g = 0 V. And this notion is also supported by the slight right-shift of Dirac (neutral) point after ATP addition. The same mechanism is also reported for DNA detection with chemical vapor deposition grown graphene film [9]. The nucleotide in both ATP and DNA can intimately interact with graphene via strong pi-pi interaction.

Conclusions

In summary, GONRs were prepared by oxidative unzipping of multi-walled carbon nanotubes. We demonstrate that the impaired graphitic structure of GONR can be effectively restored by thermal reduction in the presence of ethanol vapor. Furthermore, we show that the thin-film network devices of rGONRs exhibit high on/off ratio and are able to detect ATP molecules with high sensitivity.

Acknowledgements

We acknowledge the financial support from NNSF of China (50902071, 61076067, 61006007), the 973 Program (China, 2009CB930601), Jiangsu Province Science Foundation for Six Great Talent Peak (RLD201103), the Opening Project of State Key Laboratory of High Performance Ceramics and Superfine Microstructure (SKL201111SIC), National Research Foundation of Singapore (NRF-CRP 2-2007-02).

References

1 K. S. Novoselov, A. K. Geim, S. V. Morozov, D. Jiang, Y. Zhang, S. V. Dubonos, I. V. Grigorieva and A. A. Firsov, *Science*, 2004, **306**, 666-669.

2 X. C. Dong, Y. M. Shi, Y. Zhao, D. M. Chen, J. Ye, Y. G. Yao, F. Gao, Z. H. Ni, T. Yu, Z. X. Shen, Y. X. Huang, P. Chen and L. J. Li, *Phys. Rev. Lett.*, 2009, **102**, 135501.

3 G. Eda and M. Chhowalla, *Adv. Mater.*, 2010, **22**, 2392-2415.

4 C. Lee, X. Wei, J. W. Kysar and J. Hone, *Science*, 2008, **321**, 385-388.

5 F. Schwierz, *Nat. Nano.*, 2010, **5**, 487-496.

6 X. C. Dong, C. Y. Su, W. J. Zhang, J. W. Zhao, Q. D. Ling, W. Huang, P. Chen and L. J. Li, *Phys. Chem. Chem. Phys.*, 2010, **12**, 2164-2169.

7 M. Yang, B. G. Choi, T. J. Park, N. S. Heo, W. H. Hong and S. Y. Lee, *Nanoscale*, 2011, **3**, 2950-2956.

8 F. Schedin, A. K. Geim, S. V. Morozov, E. W. Hill, P. Blake, M. I. Katsnelson and K. S. Novoselov, *Nat. Mater.*, 2007, **6**, 652-655.

9 X. C. Dong, Y. M. Shi, W. Huang, P. Chen and L. J. Li, *Adv. Mater.*, 2010, **22**, 1649-1653.

10 Y. X. Huang, X. C. Dong, Y. M. Shi, C. M. Li, L. J. Li and P. Chen, *Nanoscale*, 2010, **2**,

1485-1488.

11 X. C. Dong, W. Huang and P. Chen, *Nanoscale Res. Lett.*, 2010, **6**, 60.

12 B. G. Choi, H. Park, M. H. Yang, Y. M. Jung, S. Y. Lee, W. H. Hong and T. J. Park, *Nanoscale*, 2010, **2**, 2692-2697.

13 A. Kaniyoor, R. Imran Jafri, T. Arockiadoss and S. Ramaprabhu, *Nanoscale*, 2009, **1**, 382-386.

14 S. Bae, H. Kim, Y. Lee, X. F. Xu, J. S. Park, Y. Zheng, J. Balakrishnan, T. Lei, H. R. Kim, Y. I. Song, Y. J. Kim, K. S. Kim, B. Ozyilmaz, J. H. Ahn, B. H. Hong and S. Iijima, *Nat. Nano.*, 2010, **5**, 574-578.

15 Y. T. Liu, Q. P. Feng, X. M. Xie and X. Y. Ye, *Carbon*, 2011, **49**, 3371-3375.

16 Y. W. Zhu, S. Murali, M. D. Stoller, K. J. Ganesh, W. W. Cai, P. J. Ferreira, A. Pirkle, R. M. Wallace, K. A. Cychosz, M. Thommes, D. Su, E. A. Stach and R. S. Ruoff, *Science*, 2011, **332**, 1537-1541.

17 L. L. Zhang, R. Zhou and X. S. Zhao, *J. Mater. Chem.*, 2010, **20**, 5983-5992.

18 M. Pumera, *Energy Environ. Sci.*, 2011, **4**, 668-674.

19 P. Reunchan and S. H. Jhi, *Appl. Phys. Lett.*, 2011, **98**.

20 J. S. Chen, Z. Y. Wang, X. C. Dong, P. Chen and X. W. Lou, *Nanoscale*, 2011, **3**, 2158-2161.

21 V. Singh, D. Joung, L. Zhai, S. Das, S. I. Khondaker and S. Seal, *Prog. Mater Sci.*, 2011, **56**, 1178-1271.

22 X. T. Jia, J. Campos-Delgado, M. Terrones, V. Meunier and M. S. Dresselhaus, *Nanoscale*, 2011, **3**, 86-95.

23 W. J. Yu, S. H. Chae, D. Perello, S. Y. Lee, G. H. Han, M. Yun and Y. H. Lee, *Acs Nano*, 2010, **4**, 5480-5486.

24 J. M. Cai, P. Ruffieux, R. Jaafar, M. Bieri, T. Braun, S. Blankenburg, M. Muoth, A. P. Seitsonen, M. Saleh, X. L. Feng, K. Mullen and R. Fasel, *Nature*, 2010, **466**, 470-473.

25 J. W. Bai, R. Cheng, F. X. Xiu, L. Liao, M. S. Wang, A. Shailos, K. L. Wang, Y. Huang and X. F. Duan, *Nat. Nano.*, 2010, **5**, 655-659.

26 J. W. Bai, X. F. Duan and Y. Huang, *Nano Lett.*, 2009, **9**, 2083-2087.

27 D. B. Shinde, J. Debgupta, A. Kushwaha, M. Aslam and V. K. Pillai, *JACS*, 2011, **133**, 4168-4171.

28 F. Cataldo, G. Compagnini, G. Patane, O. Ursini, G. Angelini, P. R. Ribic, G. Margaritondo, A. Cricenti, G. Palleschi and F. Valentini, *Carbon*, 2010, **48**, 2596-2602.

29 D. V. Kosynkin, A. L. Higginbotham, A. Sinitskii, J. R. Lomeda, A. Dimiev, B. K. Price and J. M. Tour, *Nature*, 2009, **458**, 872-875.

30 A. L. Higginbotham, D. V. Kosynkin, A. Sinitskii, Z. Z. Sun and J. M. Tour, *Acs Nano*, 2010, **4**, 2059-2069.

31 X. R. Wang and H. J. Dai, *Nat. Chem.*, 2010, **2**, 661-665.

32 C. Y. Su, Y. P. Xu, W. J. Zhang, J. W. Zhao, A. P. Liu, X. H. Tang, C. H. Tsai, Y. Z. Huang and L. J. Li, *ACS Nano*, 2010, **4**, 5285-5292.

33 X. Dong, P. Wang, W. Fang, C.-Y. Su, Y.-H. Chen, L.-J. Li, W. Huang and P. Chen, *Carbon*, 2011, **49**, 3672-3678.

34 X. Dong, B. Li, A. Wei, X. Cao, M. B. Chan-Park, H. Zhang, L.-J. Li, W. Huang and P. Chen, *Carbon*, 2011, **49**, 2944-2949.

35 D. Li, M. B. Muller, S. Gilje, R. B. Kaner and G. G. Wallace, *Nat. Nano.*, 2008, **3**, 101-105.

36 X. C. Dong, D. L. Fu, W. J. Fang, Y. M. Shi, P. Chen and L. J. Li, *Small*, 2009, **5**, 1422-1426.

37 S. Stankovich, D. A. Dikin, R. D. Piner, K. A. Kohlhaas, A. Kleinhammes, Y. Jia, Y. Wu, S. T. Nguyen and R. S. Ruoff, *Carbon*, 2007, **45**, 1558-1565.

38 X. F. Gao, J. Jang and S. Nagase, *J. Phys. Chem. C*, 2010, **114**, 832-842.

39 X. Zhang, Z. Sui, B. Xu, S. Yue, Y. Luo, W. Zhan and B. Liu, *J. Mater. Chem.*, 2011, **21**, 6494-6497.

40 C. T. M. Kwok, B. J. Reizman, D. E. Agnew, G. S. Sandhu, J. Weistroffer, M. S. Strano and E. G. Seebauer, *Carbon*, 2010, **48**, 1279-1288.

41 S. Maruyama, R. Kojima, Y. Miyauchi, S. Chiashi and M. Kohno, *Chem. Phys. Lett.*, 2002, **360**, 229-234.

42 Y. Ohno, K. Maehashi, Y. Yamashiro and K. Matsumoto, *Nano Lett.*, 2009, **9**, 3318-3322.

43 H. G. Sudibya, Q. He, H. Zhang and P. Chen, *ACS Nano*, 2011, **5**, 1990-1994.

44 X. Dong, G. Xing, M. B. Chan-Park, W. Shi, N. Xiao, J. Wang, Q. Yan, T. C. Sum, W. Huang and P. Chen, *Carbon*, 2011, **49**, 5071-5078.

45 M. Y. Han, J. C. Brant and P. Kim, *Phys. Rev. Lett.*, 2010, **104**, 056801.

46 G. Partick, T. Kathryn and G. G. David, *Phys. Rev. B*, 2010, **81**, 115409.

47 Y. X. Huang, H. G. Sudibya, D. L. Fu, R. H. Xue, X. C. Dong, L. J. Li and P. Chen, *Biosens. Bioelectron.*, 2009, **24**, 2716-2720.

48 W. R. Wang, K. R. Ratinac, S. P. Ringer, P. Thordarson, J. J. Goodng and F. Braet, *Angew.*

Chem. Int. Ed., 2010, **49**, 2114-2138.

49 Y. X. Huang, X. C. Dong, Y. X. Liu, L. J. Li and P. Chen, *J. Meter. Chem.*, 2011, **21**, 12358-12362.

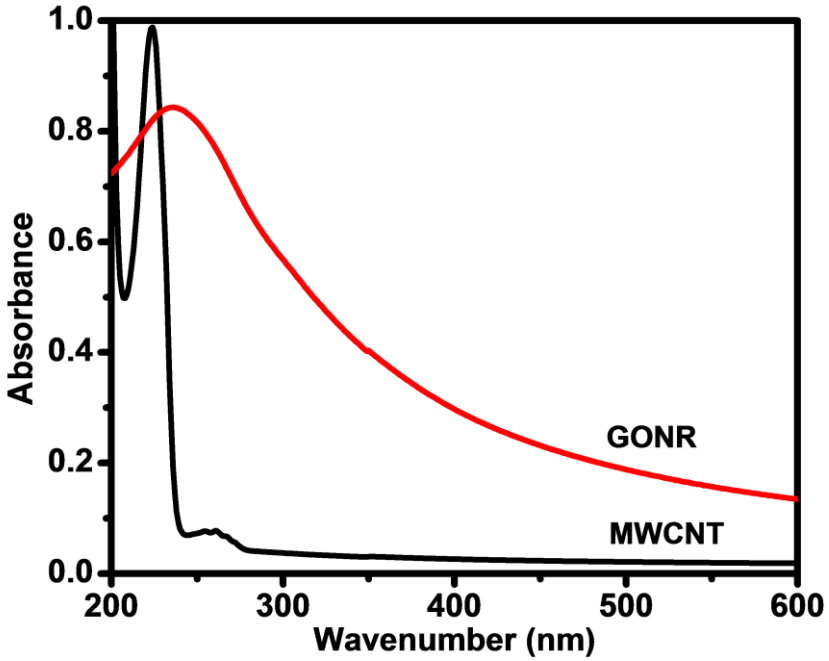

Fig. 1 UV-vis absorbance spectra of MWCNT and GONRs in water.

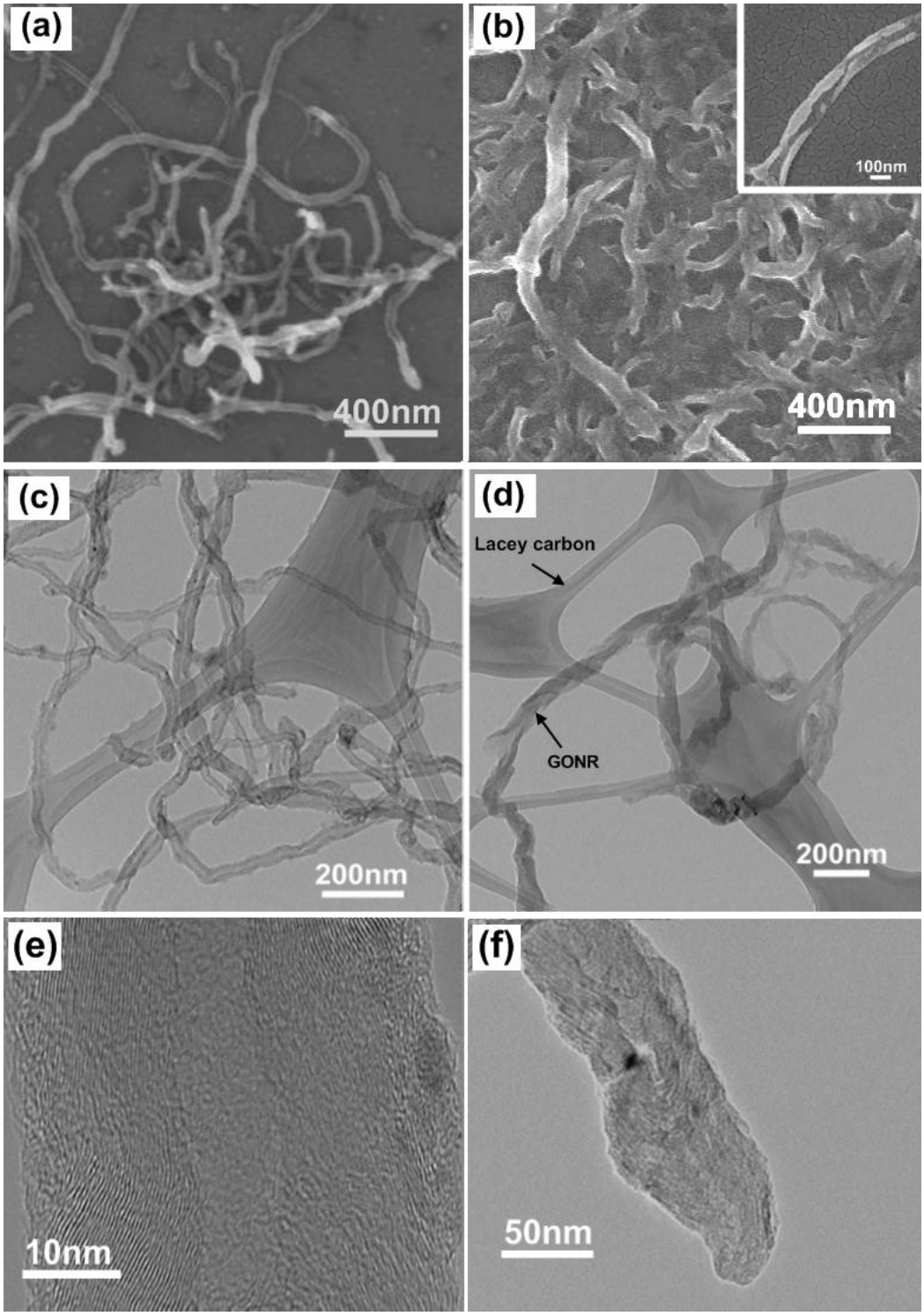

Fig. 2 (a) SEM image of MWCNTs. (b) SEM image of GONRs. The inset depicts a zoom-in SEM image of a single GONR. (c) TEM image of MWCNTs. (d) TEM image of GONRs. (e) High-resolution TEM image of MWCNT. (f) High-resolution TEM image of GONR.

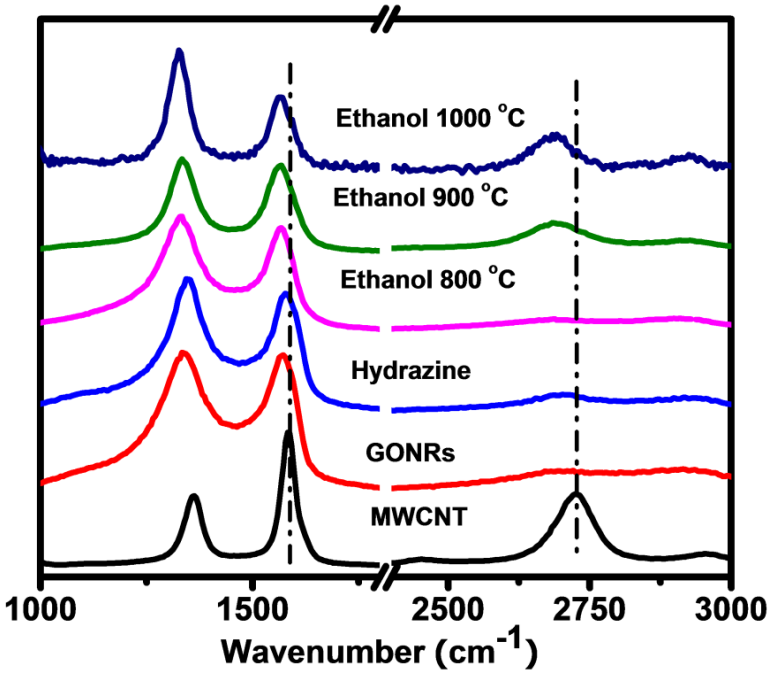

Fig. 3. Raman spectra of MWCNT, GONRs and rGONRs reduced with hydrazine vapor at 80 °C or ethanol vapor at different temperatures, respectively.

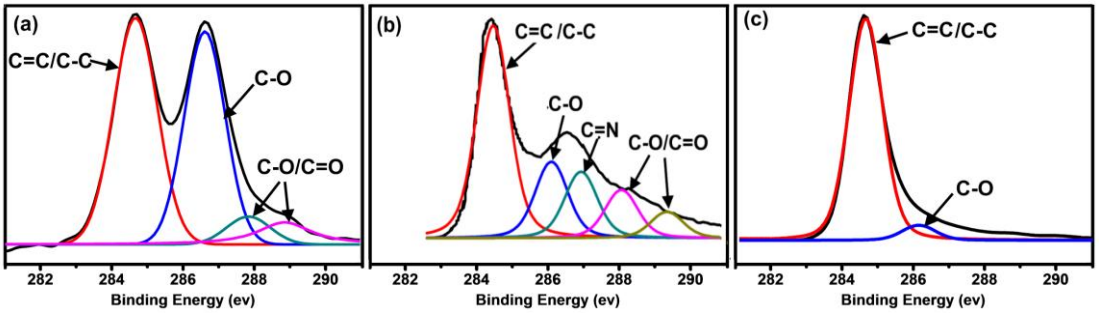

Fig. 4. XPS spectra of GONRs (a), rGONRs reduced with hydrazine vapor (b), and rGONRs reduced at 1000 ^{o}C with ethanol vapor (c).

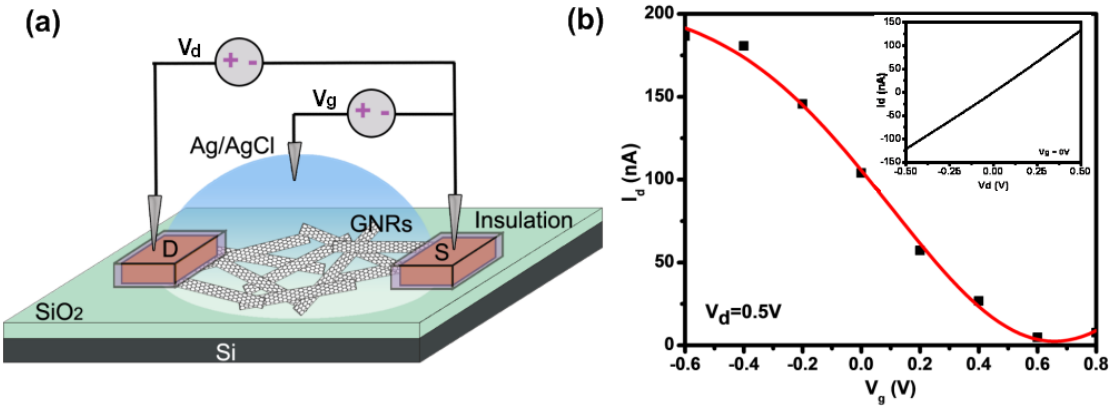

Fig. 5 (a) Schematic illustration of rGONR thin-film network device configured as liquid-gated field-effect transistor (FET) with phosphate buffer solution as the electrolyte. (b) I_d-V_g curve (source-drain current vs. gate voltage) of a typical rGONR FET biased at V_d = 0.5 V. Inset shows the I_d-V_d curve at V_g = 0 V of the same device. rGONRs were reduced at 1000 ^{o}C with ethanol vapor.

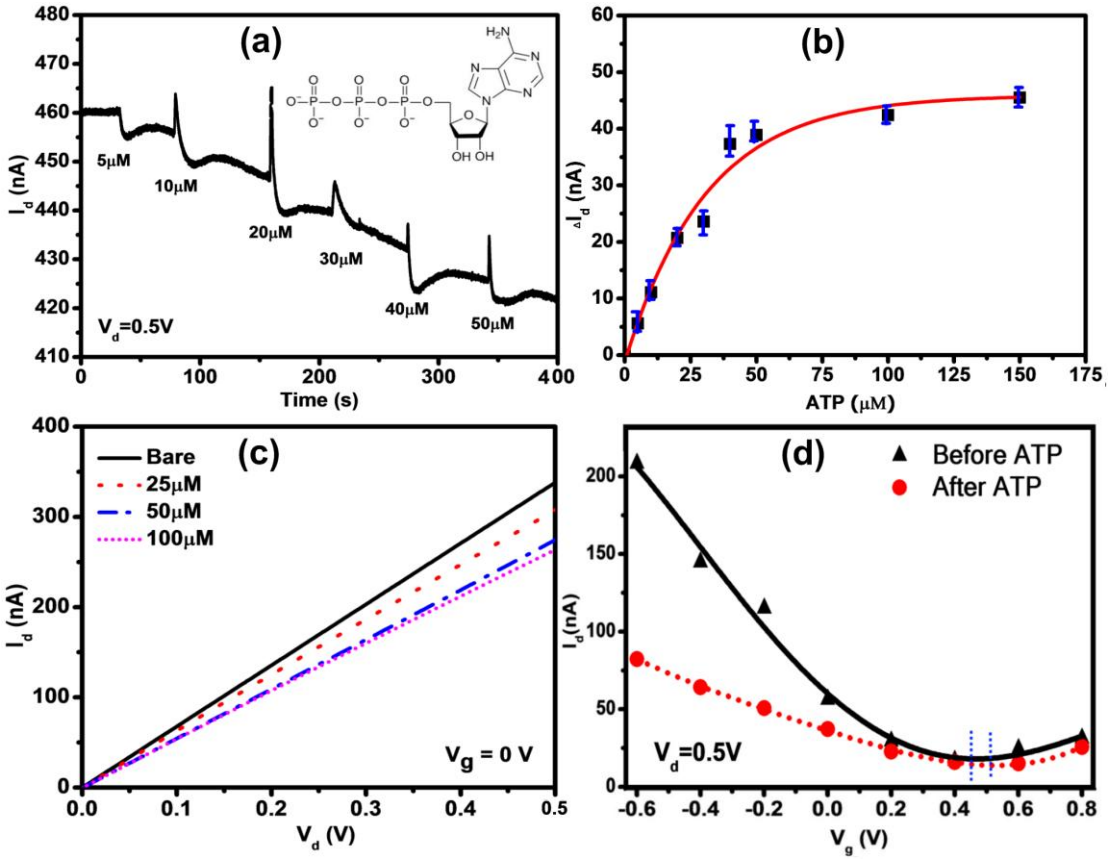

Fig. 6 (a) Real-time recording of source-drain current (I_d) of a typical rGONR thin-film device in PBS solution, at V_d = 0.5 V and V_g = 0 V. Inset shows the molecular structure of ATP. (b) The current response versus ATP concentration (n = 3 devices, and the error bars indicates the standard deviation). (c) The changes of I_d-V_d curves of rGONRs device upon addition of ATP with different concentrations. (d) I_d-V_g curves of a rGONRs network device before and after the addition of 100 μM ATP.